Electronic Supplementary Material (ESI) for Dalton Transactions.

Thermal and protonation-induced electron transfer coupled spin transition in discrete [Fe_2Co_3] Prussian Blue Analogue

Jyoti Yadav[a], Monojit Nandi[a], Ranjan Kharel[a], Moubani Mukherjee[a], Sanjit Konar[*a]

a. Department of Chemistry, Indian Institute of Science Education and Research Bhopal, Bhauri, Bhopal-462066, Madhya Pradesh, India
Email: skonar@iiserb.ac.in

Table of Contents

1. Experimental Details:

1.1. Materials:

The metal salts were purchased from Aldrich and used as received. All other chemicals 4-(trifluoromethyl)aniline, Sodium methoxide and 2-cyanopyridine were procured from S.D. Fine Chemicals, India. All solvents used were at least reagent grade. All the reactions were performed in air unless otherwise stated.

1.2. Synthetic procedures:

1.2.1. Synthesis of ligand (L) (Z)-N'-(4-(trifluoromethyl)phenyl)picolinimidamide:

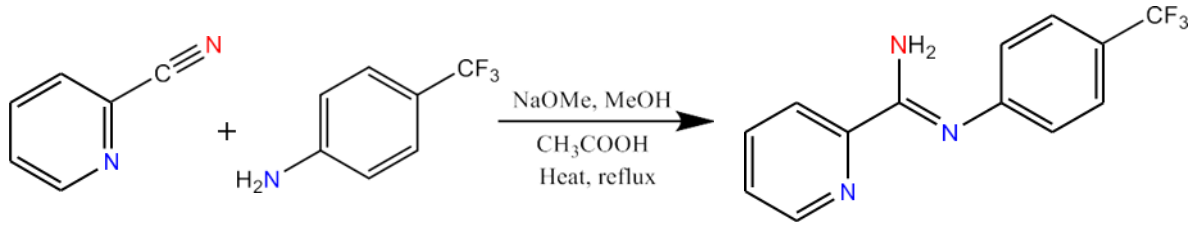

Scheme 1. Synthesis of ligand(L).

The ligand was prepared by reacting 2-cyanopyridine and 4-(trifluoromethyl)aniline in one-pot synthesis. An excess amount of sodium methoxide (0.35 g, 7 mmol) was dissolved in 25 ml of CH_3OH and heated at 50°C for ~10 minutes to obtain a clear solution. To this reaction mixture, 2-cyanopyridine (0.48 mL, 5 mmol) was added slowly and refluxed at 70 °C for 1 hour. 4-(trifluoromethyl)aniline (0.63 mL, 5 mmol) was added followed by addition of 0.1 mL of glacial acetic acid in the reaction mixture. The reaction mixture was refluxed for overnight. The pale-yellow solution was filtered and dried by rotatory evaporator. The product was washed with diethyl-ether and hexane several times and left for evaporation. Pale yellow crystals of the product was obtained with a yield of 60 %.

IR data (cm^{-1}): ν_{N-H} = 3486.33; ν_{C-H} = 2926.53; $\nu_{C=N}$ = 1637.47; ν_{C-F} = 1241.34.

1.2.2. Synthesis of complex $\{[Co(L)_2]_3[Fe(CN)_6]_2 \cdot 20H_2O$ ($1 \cdot 20H_2O$):

26.52 mg (0.1 mmol) of ligand (L) was dissolved in 5 mL of CH_3OH into which 17 mg (0.05 mmol) of $Co(BF_4)_2 \cdot 6H_2O$ was added and stirred for 30 minutes. To this solution, 5 mL aqueous solution of potassium ferricyanide (16.46 mg, 0.05 mmol) was added and then heated at 50 ˚C for another 1 hour. The resultant mixture was then filtered and left for slow evaporation

at room temperature. Dark blue crystals suitable for single-crystal X-ray diffraction measurement were obtained after one week. The crystals were washed with water, dried and used for further characterization and other physical measurements. Elemental analysis: experimental (calculated for $C_{90}H_{100}Co_3F_{18}Fe_2N_{30}O_{20}$): C, 42.82% (42.35%); H, 3.59% (3.95%); N, 16.39% (16.46%).

IR data (cm^{-1}): ν_{N-H} = 3339; ν_{C-H} = 3108; ν_{CN} = 2141, 2113, 2058, 2047, 2027, and $\nu_{C=C}$ = 1437.

1.3. Physical measurements:

1.3.1. Crystal Data Collection and Structure Determination:

Intensity data were collected on a 'Bruker D8-venture' diffractometer using a graphite monochromated MoKα radiation (λ = 0.71073) at 140 K. Data collections were performed using ϕ and ω scan. Olex2 was used as the graphical interface and the structures were solved with olex2.solve structure solution program using Charge Flipping and refined with the ShelXL refinement package using Least-Squares minimisation. All non-hydrogen atoms were refined anisotropically.[1] Octahedral distortion parameters were calculated by using software "Octadist".[2]

1.3.2. Squid magnetometry:

The magnetic study has been performed using a SQUID-VSM magnetometer. All samples were ground properly before measuring magnetic moment vs. temperature data, to minimize the reorientation of the crystalline particles under the applied DC field. All the measurement has been performed with an applied DC field of 10000 Oe from the 2 K to 300 K temperature range. The high temperature susceptibility measurement was performed by using oven module between 300 K and 430 K. The measured values were corrected for the experimentally measured contribution of the sample holder and the derived susceptibilities were corrected for the diamagnetism of the samples, estimated from Pascal's tables.

1.3.3. Differential scanning calorimetry:

The Differential Scanning Calorimetric study was performed on Perkin-Elmer, Pyris 6 type DSC 4000 instrument. Data collected and baseline correction was done using software version 11.0.0.0449. The data measurement was taken at a scan rate of 5 K/min.

1.3.4. FT-Infrared spectroscopy:

FT-IR spectra were recorded by using a Perkin-Elmer Spectrum BX Spectrometer between 4000 cm^{-1} - 400 cm^{-1} wavenumber.

1.3.5. ^{1}H-NMR spectroscopy:

^{1}H-NMR spectroscopy measurement was performed on CD_3OD solution of ligand and the complex using Bruker's AVANCE-III 500 MHz NMR spectrometer. The data analysis was done by using MestReNova-15.0.1-35756 software.

1.3.6. Thermogravimetric analysis:

The Thermogravimetric analysis was performed on a Perkin-Elmer instrument at a scan rate of 5 K/min under N_2 atmosphere.

1.3.7. UV-visible spectroscopy:

The solution phase UV-Visible spectroscopic data was collected using Cary 100 instrument using Scan Software Version 4.20(468) scanning between wavelength 200 nm to 800 nm at 298 K with subsequent addition of trifluoroacetic acid into the methanolic solution of the complex. While the solid state UV-Visible spectroscopic data was collected using Shimadzu UV-2600i instrument between wavelength 200 nm to 1200 nm.

1.3.8. Cyclic voltammetry:

The electrochemical study of the sample was measured by using VersaSTAT-3 instrument using software VersaStudio. The study was done by using three-electrode system consisting of glassy carbon as working electrode, Pt wire as a counter electrode and Ag/AgCl electrode as a reference electrode. 5×10^{-4} M concentration of **1**·$20H_2O$ was used for the data collection and 0.1 M of $[N(Bu)_4]PF_6$ was used as supporting electrolyte in anhydrous methanol. The scan range for the sample solutions were from 0 V to -0.40 to +1.2 V. The scanning cycle was performed anodically. The measurement was performed at a scan rate of 0.05 V/s at 298 K. For $K_3[Fe(CN)_6]$, 1×10^{-4} M concentration in water was used and the measurement was performed using same three-electrode system with 0.1 M KCl as the supporting electrolyte. The scan range for the sample solutions were taken from 0 V to -0.05 to +0.6 V with a scan rate of 0.05 V/s at 298 K.

2. Result and Discussion:

2.1. Crystal structure determination:

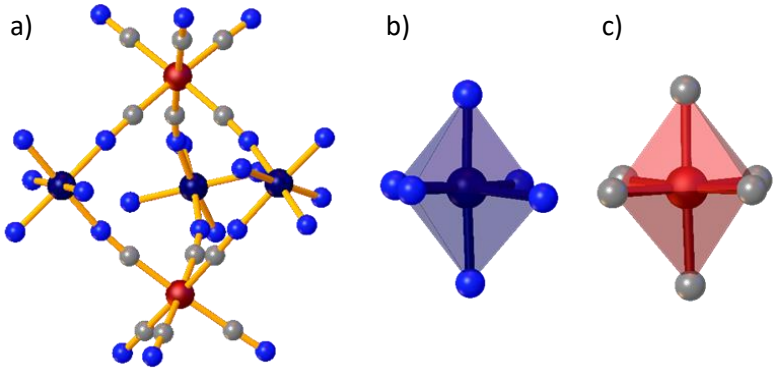

Figure S1. (a) Simplified structure and (b) and (c) coordination environment around Co and Fe centres, respectively, in complex **1**·20H_2O. Colour code: brown (Fe), dark blue (Co), light blue (N) and grey (C).

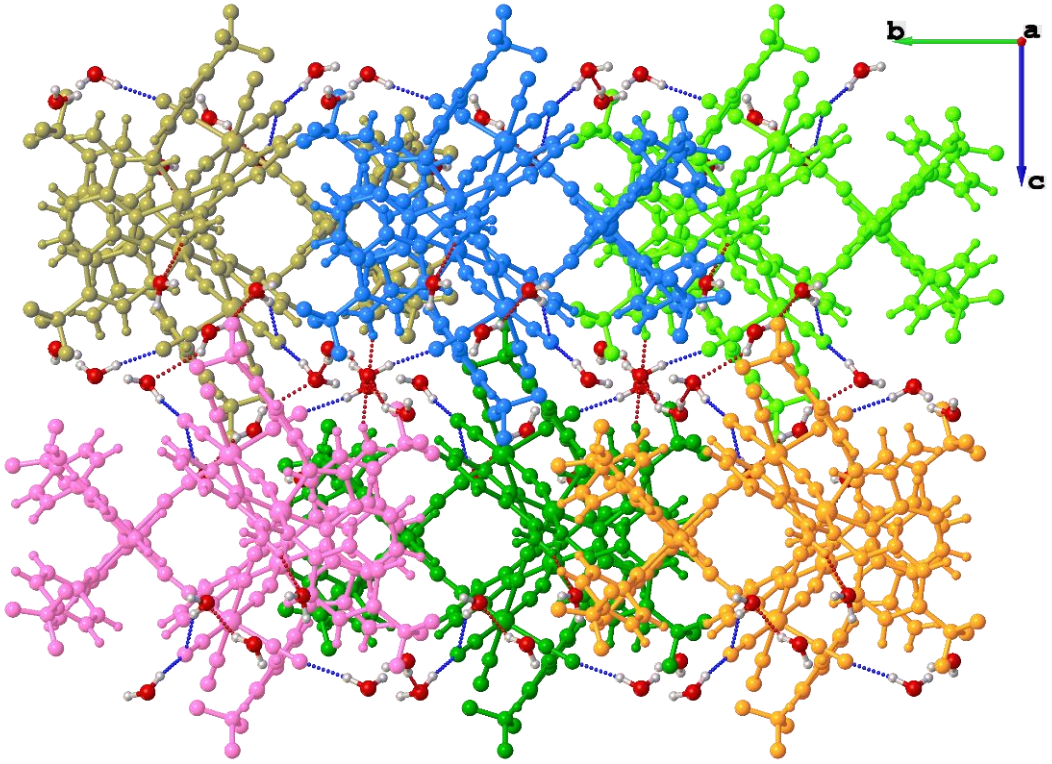

Figure S2. Crystal-packing along a-axis showing intermolecular hydrogen bonding interactions in complex **1**·20H_2O. Each pentanuclear [Fe_2Co_3] units are represented with different colours.

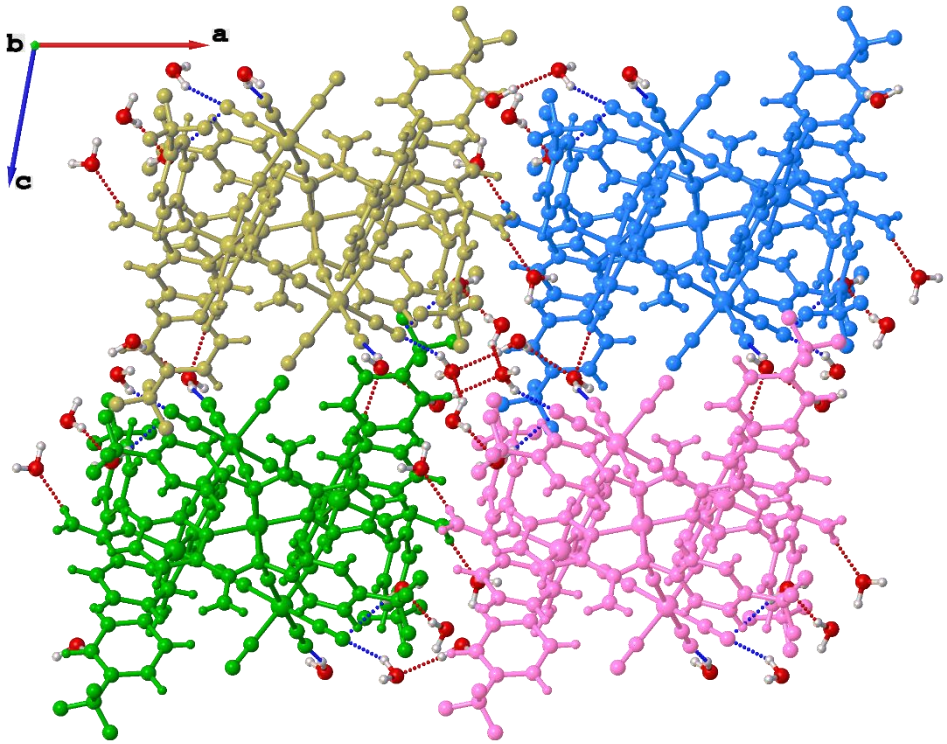

Figure S3. Crystal-packing along b-axis showing intermolecular hydrogen bonding interactions in complex **1**·20H_2O. Each pentanuclear [Fe_2Co_3] units are represented with different colours.

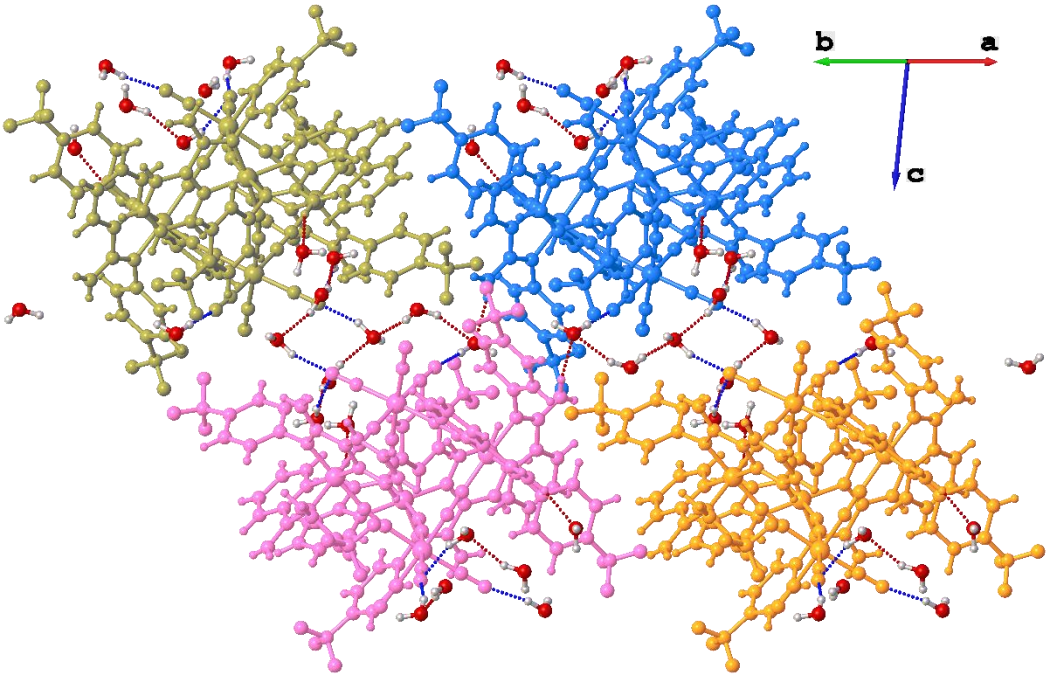

Figure S4. Crystal-packing along abc-dihedral angle showing intermolecular hydrogen bonding interactions in complex **1**·20H_2O. Each pentanuclear [Fe_2Co_3] units are represented with different colours.

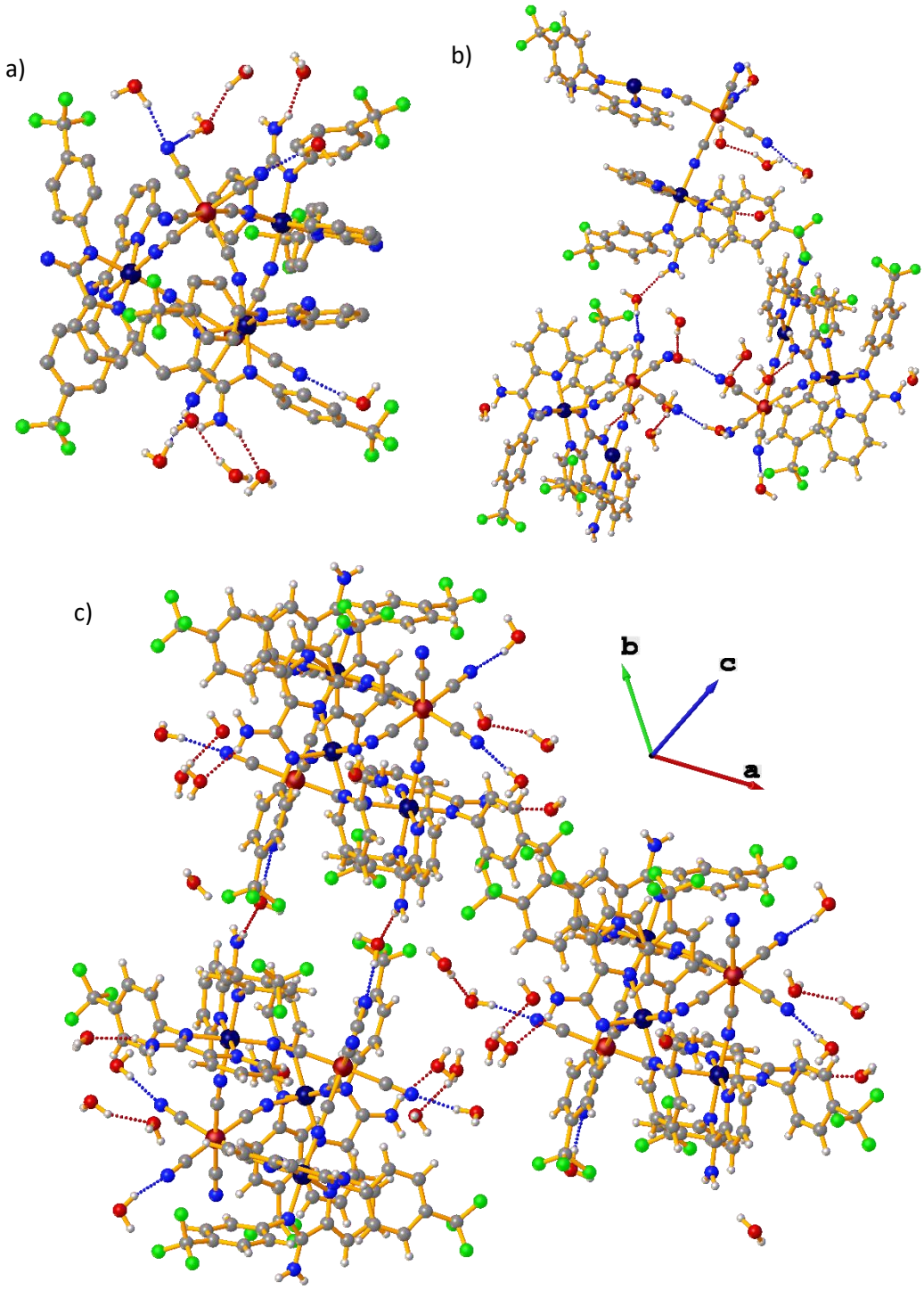

Figure S5. H-bonding interactions between solvent molecules and (a) $[Fe_2Co_3]$ complete unit, (b) neighbouring asymmetric units and (c) neighbouring pentanuclear $[Fe_2Co_3]$ units.

2.2. Crystallographic details:

Table S1. Crystallographic data for complex **1**·20H_2O (with masked solvents).

Empirical formula	$C_{45}H_{42}Co_{1.5}F_9FeN_{15}O_6$
Formula weight	1204.18
Temperature/K	140.0
Crystal system	monoclinic
Space group	C2/c
a/Å	28.9299(12)
b/Å	19.9584(12)
c/Å	23.2361(11)
α/°	90
β/°	100.411(2)
γ/°	90
Volume/$Å^3$	13195.5(12)
Z	8
$\rho_{calc}g/cm^3$	1.212
μ/mm^{-1}	0.667
F(000)	4900.0
Crystal size/mm^3	0.25 × 0.13 × 0.04
Radiation	MoKα (λ = 0.71073)
2Θ range for data collection/°	4.798 to 51.926
Index ranges	-35 ≤ h ≤ 35, -24 ≤ k ≤ 24, -28 ≤ l ≤ 28
Reflections collected	99634
Independent reflections	12726 [R_{int} = 0.0684, R_{sigma} = 0.0412]
Data/restraints/parameters	12726/0/717
Goodness-of-fit on F^2	1.030
Final R indexes [I>=2σ (I)]	R_1 = 0.0461, wR_2 = 0.1187
Final R indexes [all data]	R_1 = 0.0592, wR_2 = 0.1277
Largest diff. peak/hole / e $Å^{-3}$	0.59/-0.51

Table S2. Bond lengths around the Fe and Co centres in complex **1**·20H_2O.

Atoms		Bond length(Å)
Co1	N4	1.927(2)
Co1	N8	1.886(2)
Co1	N7	1.894(2)
Co1	N3	1.927(2)
Co1	N1	1.934(2)
Co1	N6	1.938(2)
Fe1	C28	1.894(3)
Fe1	$C27^1$	1.901(3)
Fe1	C32	1.899(3)
Fe1	C30	1.920(3)
Fe1	C29	1.909(3)
Fe1	C31	1.913(3)
Co2	N13	1.938(2)
Co2	$N13^1$	1.938(2)
Co2	N15	1.930(2)
Co2	$N15^1$	1.930(2)
Co2	N12	1.878(3)
Co2	$N12^1$	1.878(3)

Table S3. Distortion parameters[2] for Fe and Co centres in complex **1**·20H_2O.

Metal centre	<D> (Å)	Z (Å)	Δ	Σ (°)	Θ (°)
Co1	1.9178	0.111647	0.000111	32.0493	115.4752
Co2	1.9154	0.149127	0.000193	36.0423	122.8782
Fe1	1.9059	0.047246	0.000021	15.4210	38.2567

Table S4. Bond angles around Fe and Co centres in complex **1**·20H_2O.

Atoms			Bond angles (°)	Atoms			Bond angles (°)
N4	Co1	N3	90.16(9)	C28	Fe1	$C27^1$	87.77(10)
N4	Co1	N1	93.79(9)	C28	Fe1	C32	87.13(11)
N4	Co1	N6	82.11(9)	C28	Fe1	C30	92.22(12)
N8	Co1	N4	175.77(9)	C28	Fe1	C29	90.10(12)
N8	Co1	N7	90.19(9)	C28	Fe1	C31	176.90(11)
N8	Co1	N3	89.82(9)	$C27^1$	Fe1	C30	178.03(12)
N8	Co1	N1	90.40(9)	$C27^1$	Fe1	C29	90.50(12)
N8	Co1	N6	93.68(9)	$C27^1$	Fe1	C31	89.33(11)
N7	Co1	N4	90.14(9)	C32	Fe1	$C27^1$	88.52(11)
N7	Co1	N3	175.86(10)	C32	Fe1	C30	89.51(12)
N7	Co1	N1	93.67(9)	C32	Fe1	C29	177.10(12)
N7	Co1	N6	90.16(9)	C32	Fe1	C31	91.70(13)
N3	Co1	N1	82.19(10)	C29	Fe1	C30	91.47(12)
N3	Co1	N6	93.97(9)	C29	Fe1	C31	91.02(13)
N1	Co1	N6	174.40(9)	C31	Fe1	C30	90.64(12)
$N13^1$	Co2	N13	173.10(14)				
$N15^1$	Co2	N13	93.30(10)				
N15	Co2	$N13^1$	93.30(10)				
N15	Co2	N13	81.86(10)				
$N15^1$	Co2	$N13^1$	81.86(10)				
N15	Co2	$N15^1$	91.40(15)				
$N12^1$	Co2	N13	90.20(10)				
$N12^1$	Co2	$N13^1$	94.66(11)				
N12	Co2	N13	94.66(11)				
N12	Co2	$N13^1$	90.20(10)				
N12	Co2	$N15^1$	89.20(10)				
N12	Co2	N15	176.50(11)				
$N12^1$	Co2	N15	89.20(10)				
$N12^1$	Co2	$N15^1$	176.49(11)				
$N12^1$	Co2	N12	90.41(14)				

Table S5. Hydrogen bonding interactions considering maximum 2.9 Å bond distances and minimum 120° bond angles.

Atoms	Bond length (Å)
N2…O4	2.898
N5…O6	2.823
O6…N5	2.799
O1…N10	2.817
O5…O6	2.899
O5…O1	2.766
O3…O2	2.829

2.3. Solid-state UV-visible spectroscopy study:

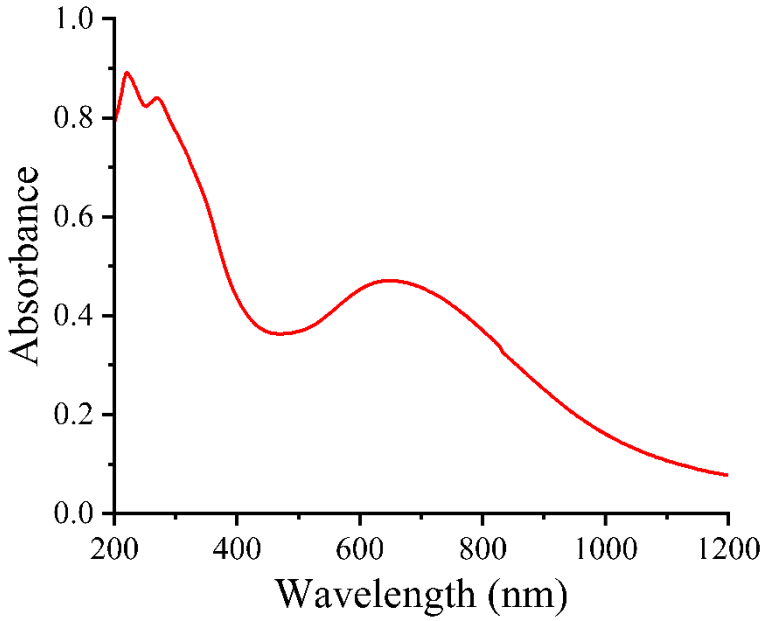

Figure S6. Solid-state UV-visible spectrum of the complex **1**·20H_2O.

2.4. Magnetic study:

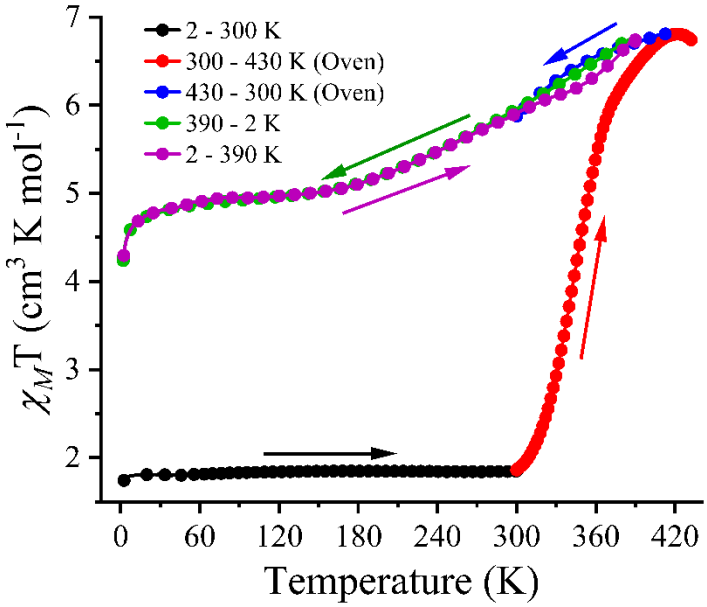

Figure S7. $\chi_M T$ *vs.* T plot of the complex **1**·20H_2O (between 2 - 300 - 430 K) and **1** (between 430 - 300 K and 390 - 2- 390 K) at a constant magnetic field of 10000 Oe.

2.5. Differential scanning calorimetric study:

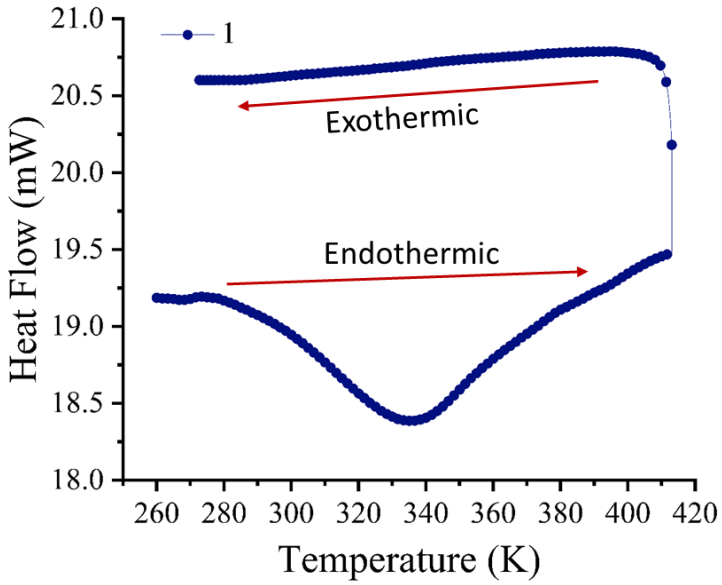

Figure S8. DSC study of complex **1**·20H_2O.

2.6. Infrared spectroscopic studies with acid addition:

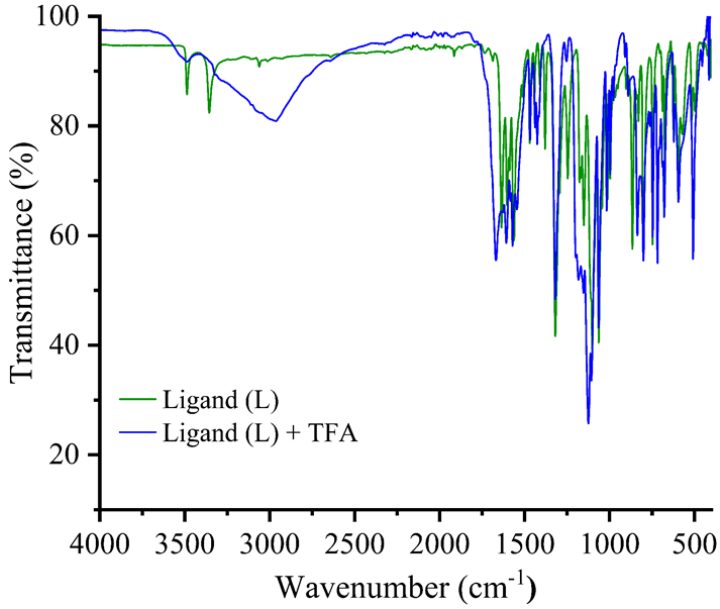

Figure S9. IR of ligand (L) before (green) and after (blue) addition of triflouroacetic acid (TFA).

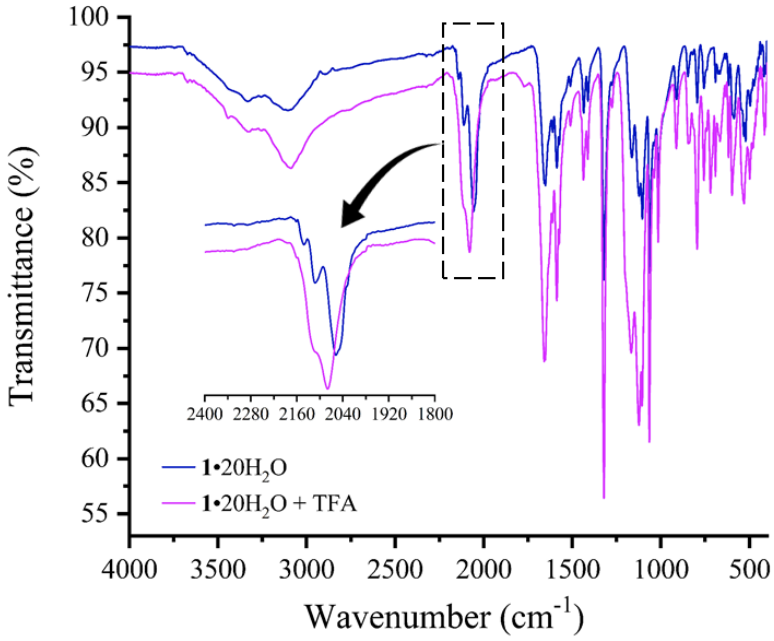

Figure S10. IR of complex **1**·20H_2O before (blue) and after (magenta) addition of TFA.

The complex **1**·20H_2O gives ν_{CN} stretching frequencies at 2141, 2113, 2058, 2047 and 2027 cm^{-1} corresponds to the presence of $[Fe^{II}_{LS}(\mu CN)Co^{III}_{LS}]$ as well as $[Fe^{III}_{LS}(\mu CN)Co^{II}_{HS}]$.[3] Upon addition of the trifluoroacetic acid (TFA), the ν_{CN} stretching frequencies shifts to higher wavenumber 2114 and 2080 cm^{-1} corresponds to the presence of only $[Fe^{III}_{LS}(\mu CN)Co^{II}_{HS}]$ configurations. The ν_{NH2} stretching frequency at 3339 cm^{-1} shifts to lower wavenumber 3327 cm^{-1} indicating protonation at the $–NH_2$ site forming $–^{+}NH_3$.[4]

Similarly, the ν_{NH2} stretching frequency of the ligand shifts to a higher wavenumber upon addition of TFA, justifying the protonation at $–NH_2$ sites.

2.7. ^{1}H-NMR study:

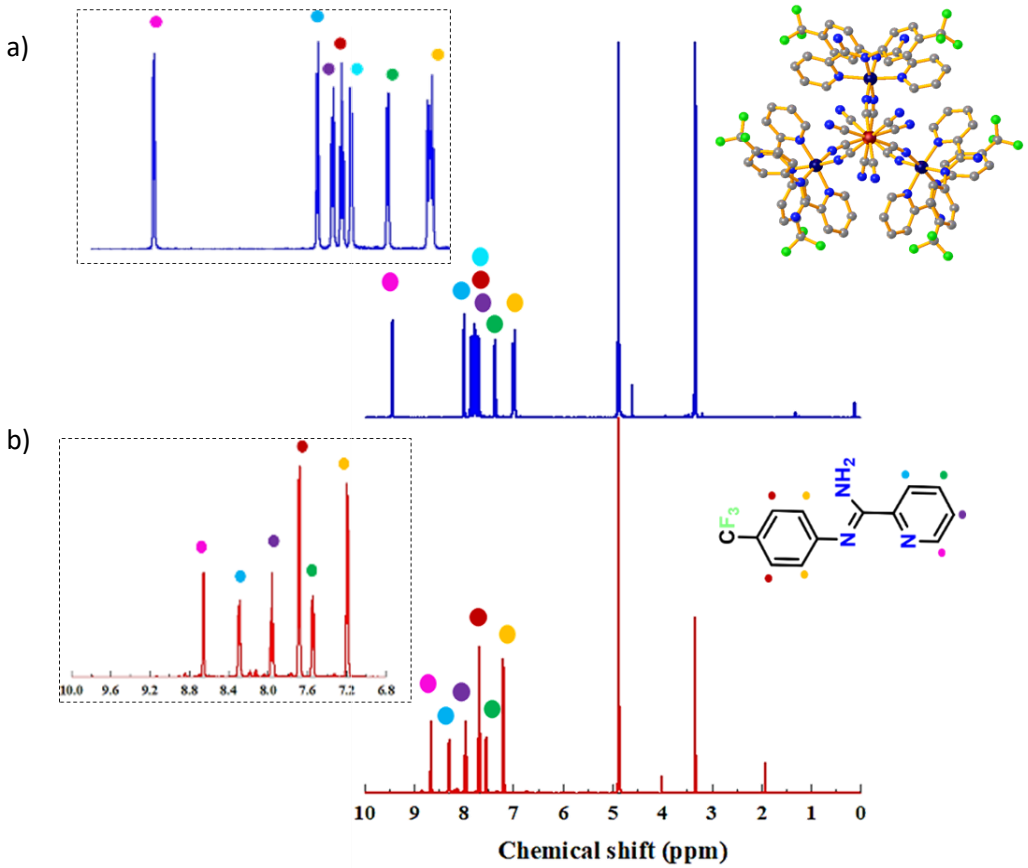

Figure S11. ^{1}H-NMR shift of (a) complex **1**·20H_2O and (b) ligand (L) in CD_3OD showing peaks for the labelled protons. Insets shows the enlarged spectra between 6.8 to 10 ppm.

Table S6. ^{1}H-NMR shift observed in ligand and in complex **1**·20H_2O.

δ (ppm) for L	δ (ppm) for Complex 1	^{1}H-NMR shift of ligand after complex formation
8.65	9.43	downfield
8.29	7.98	upfield
7.956	7.85	upfield
7.68	7.77	downfield
-----	7.68	new peak
7.54	7.36	upfield
7.19	6.97	upfield

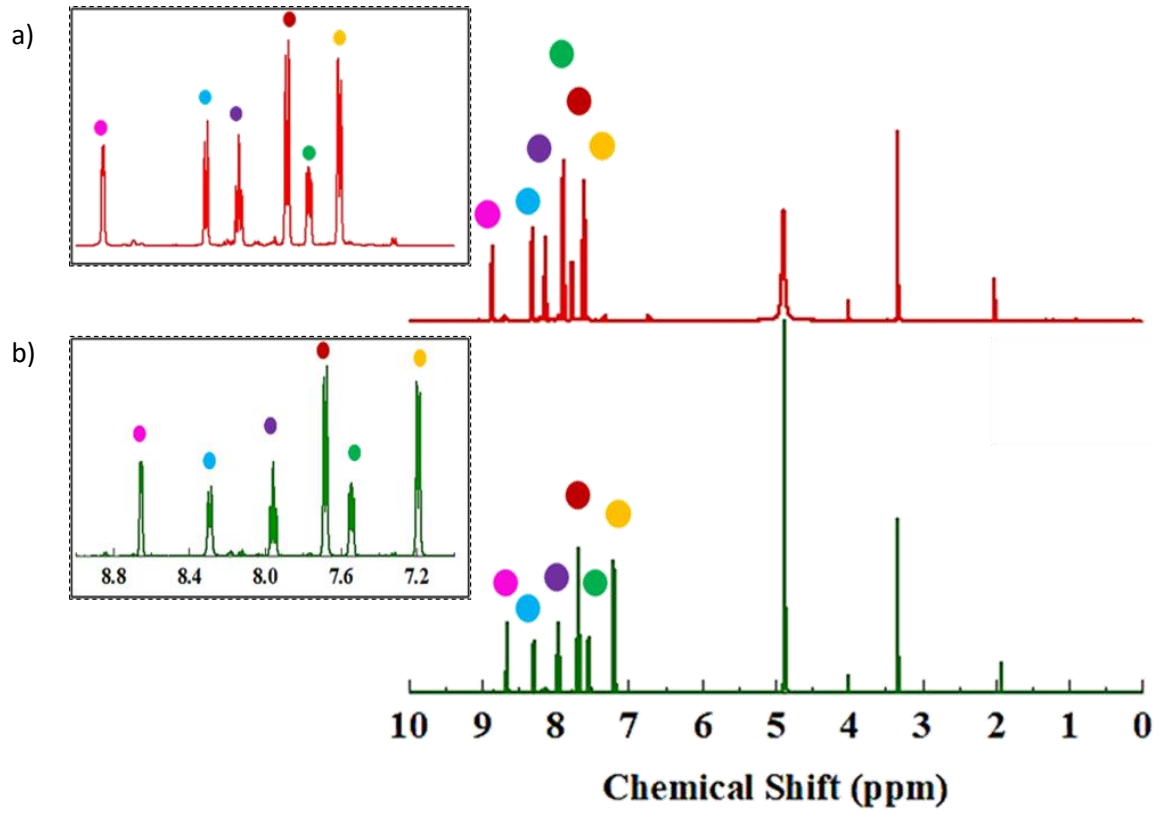

Figure S12: ^{1}H-NMR NMR shift comparison of ligand (L) (a) after and (b) before TFA addition in CD_3OD. Enlarged spectra corresponding to the labelled protons between 6.8 to 9 ppm is shown in the insets.

Table S7. ^{1}H-NMR shift comparison of ligand (L) before and after TFA addition.

δ (ppm) for L	δ (ppm) for L after TFA addition	Nature of shift after TFA addition
8.65	8.85	downfield
8.29	8.31	downfield
7.956	8.137	downfield
7.68	7.88	downfield
7.54	7.76	downfield
7.19	7.6	downfield

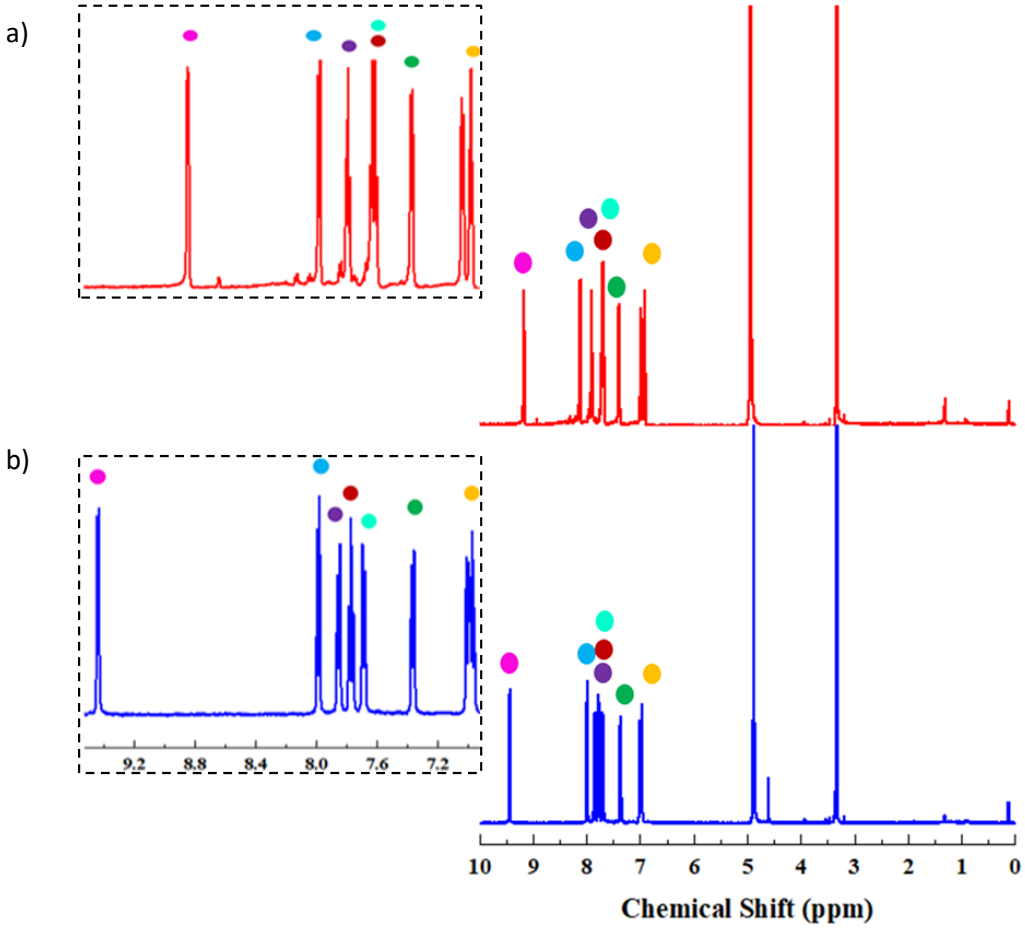

Figure S13. ^{1}H-NMR shift of complex **1** (a) after and (b) before TFA addition in CD_3OD. Enlarged spectra corresponding to the labelled protons between 6.8 to 9 ppm is shown in the insets.

Table S8. ^{1}H-NMR shift comparison of complex **1**·20H_2O before and after TFA addition.

δ (ppm) for Complex 1	**δ (ppm) for complex 1**·20H_2O **after TFA addition**	**Nature of shift after TFA addition**
9.43	9.18	upfield
7.98	8.11	downfield
7.85	7.72	upfield
7.77	7.88	downfield
7.68	7.67	upfield
7.364	7.38	downfield
6.97	6.91	upfield

NMR spectra of ligand (**L**) and complex **1**·20H_2O were recorded in CD_3OD at 298 K. A comparative ^1H NMR spectra of **L**, and **1**·20H_2O are presented in Figure S11 and changes in chemical shift value after complex formation are highlighted in Table S6. All the aromatic protons of **L** resonate in the expected range of 7.19-8.65 ppm, which shifted after complex formation and resonates in the range of 6.97-9.43 ppm. Interestingly, it is found that protons highlighted in pink and brown colour are shown downfield, and other protons are shown upfield due to the coordination of both the nitrogen atoms of **L** to Co metal center of **1**·20H_2O. The chemical shift value of the proton highlighted in pink colour resonates at 8.66 ppm (in **L**), which shifted downfield to 9.44 ppm (in **1**·20H_2O) due to the deshielding effect in the metal complex. The effect of the addition of TFA in ^1H NMR spectra of **L** is presented in Figure S12 and the changes in chemical shift values before and after TFA addition are summarized in Table S7. It is found that, after protonation, all the aromatic protons are deshielded and appear in the range of 7.6-8.85 ppm.

Similarly, the effect of TFA addition to the complex **1**·20H_2O is highlighted in Figure S15 and data on chemical shift value is summarised in Table S8. Surprisingly, it was found that few of the aromatic protons showed upfield shifting after complex formation and appeared in the range of 6.91-9.18 ppm. From Figure S13 and Table S8, it is concluded that protons highlighted as pink, navy blue, orange and brown colours are shown upfield and other protons are shown downfield. After the addition of TFA, these changes happen due to the protonation of the free amine group present in the system. After protonation, it creates a positive charge on the nitrogen atom of amine, increases electrophilicity, and changes the electronic environment in the entire system. As a result, the redox potential of the metal complex changes, which is responsible for metal-to-metal charge transfer-induced spin transition in the entire system.

2.8. Thermogravimetric analysis:

Thermogravimetric analysis (TGA) of complex **1**·20H_2O is carried out in N_2 atmosphere at heating rate of 5 °C /min. The TGA data reveals a gradual loss of 14.5 % of its total sample weight in the range of 30 °C - 100 °C which can be attributed to the loss of approximately 20 water molecules. Above 241 °C, the weight loss corresponds to the disintegration of the structural framework.

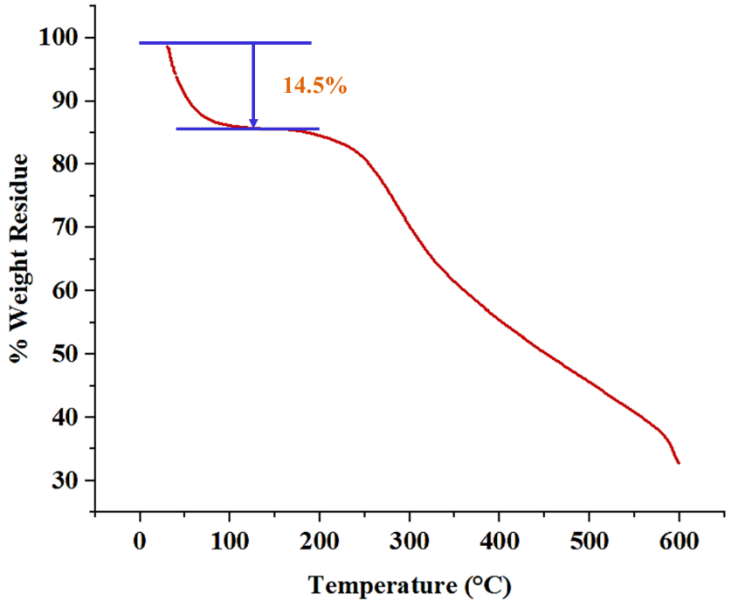

Figure S14. TGA of complex **1**·20H_2O.

2.9. Cyclic voltametric study:

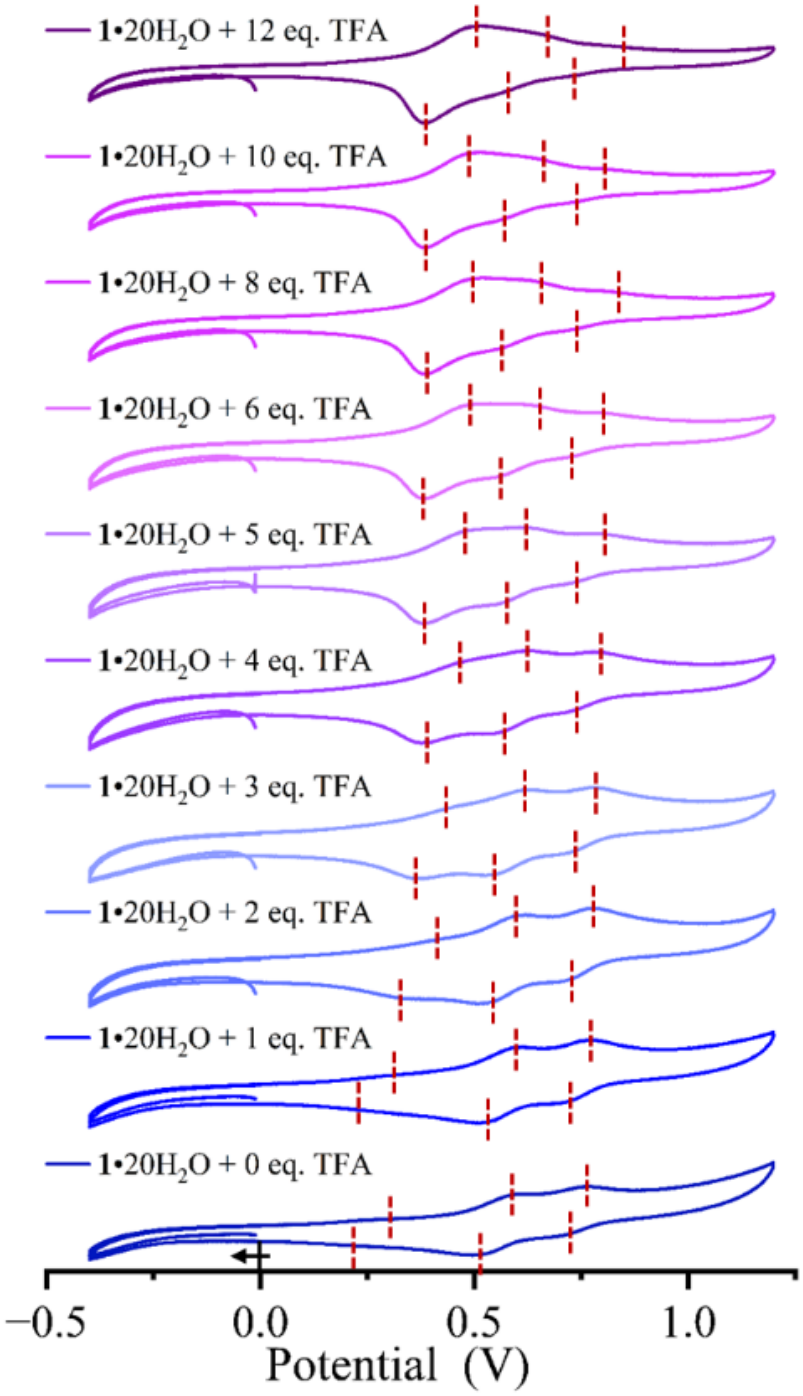

Figure S15. Electrochemical spectra with subsequent addition of TFA into the methanolic solution of complex **1**·20H_2O.

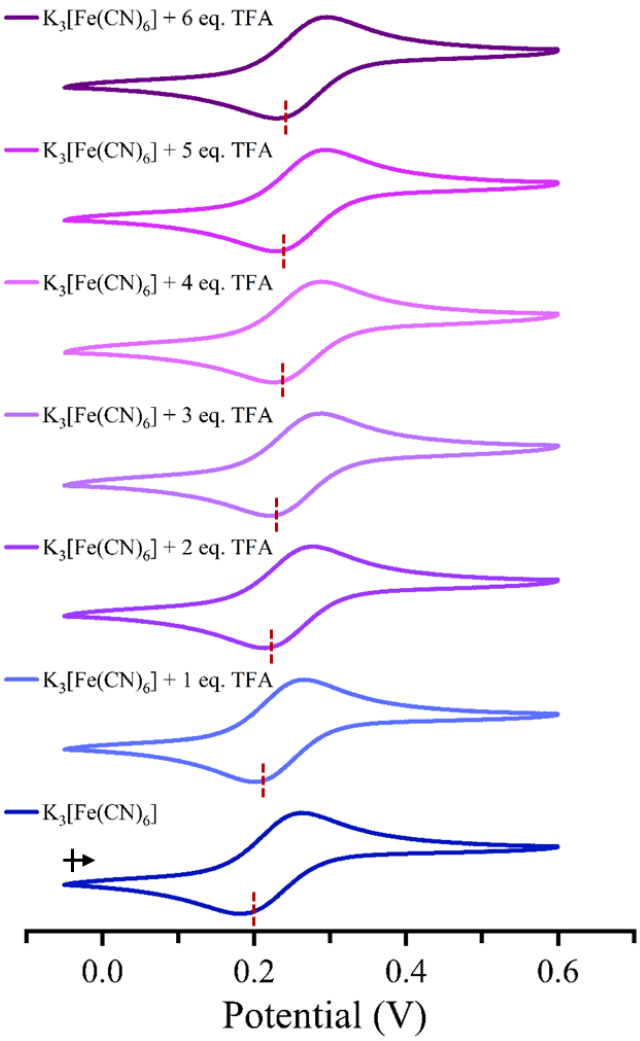

Figure S16. Electrochemical spectra with subsequent addition of TFA into the aqueous solution of $K_3[Fe(CN)_6]$.

3. References:

1. O. V. Dolomanov, L. J. Bourhis, R. J. Gildea, J. A. K. Howard, and H. Puschmann, J. Appl. Cryst., 2009, **42**, 339-341.
2. R. Ketkaew et al. Octadist. 2019.
3. C. P. Berlinguette, A. Dragulescu-Andrasi, A. Sieber, H. U. Gudel, C. Achim, K. R. Dunbar, *J. Am. Chem. Soc.*, 2005, **127**, 6766-6779.
4. J. M. Price, M. W. Crofton and Y. T. Lee, *J. Phys. Chem*., 1991, **95**, 2182-2195.